RJC

RASĀYAN *J. Chem.*
Vol. 17 | No. 3 |1146-1153| July - September | 2024
ISSN: 0974-1496 | e-ISSN: 0976-0083 | CODEN: RJCABP
http://www.rasayanjournal.com
http://www.rasayanjournal.co.in

THE SYNTHESIS OF A COPPER (II) OXIDE (CUO)/ REDUCED GRAPHENE OXIDE (RGO) NANOCOMPOSITE USING A HYDROTHERMAL METHOD FOR USE IN BIOLOGICAL APPLICATIONS

Ravi Kota[1,✉], Jayarangarao Prathipati[1], Matcha Sowbhagya Lakshmi[2], Yaddanapudi Venkata Bhaskara Lakshmi[1] and Narasimhulu Tamminana[1]

[1]Baba Institute of Technology and Sciences, JNTUGV, Visakhapatnam-530048, Andhra Pradesh, India
[2]JNTU, Vizianagaram -535003, Andhra Pradesh, India
✉Corresponding Author: ravibitsvizag@gmail.com

ABSTRACT

This study focuses on the degradation of pollutants through photocatalysis involves utilizing light-induced catalytic processes to break down harmful substances. The CuO/RGO nanocomposite is employed for visible light-induced photocatalytic degradation regarding pollutants such as 2-nitrophenol (2-NP) and 4-nitrophenol (4-NP). The nanocomposite was synthesized through a green and straightforward hydrothermal method in a solvent-free environment. The resulting structure and morphology of the product can be characterized as follows: composite was analyzed using FESEM and TEM, while elemental analysis (EDS) was confirmed. The existence of copper, oxygen, and carbon is evident. FTIR spectra revealed characteristics. The peaks detected within the 600-400 cm^{-1} range confirm the development of monoclinic CuO. Nevertheless, the composites exhibited significant agglomeration attributed to the presence of iron oxide and silver. Continued exploration of the ternary nanocomposite involves further investigation. Morphology was conducted through TEM at magnifications of 50 and 100 nm, highlighting agglomeration issues. The composite exhibited superior degradation of 4-NP compared to pure CuO, achieving complete degradation of 4-NP, while CuO alone achieved only 72%.

Keywords: Photocatalytic Degradation; Antimicrobial Activity, Nanocomposite, Biochemical Applications, Cuo/RGO.

RASĀYAN*J. Chem.*, Vol. 17, No.3, 2024

INTRODUCTION

Water pollution is caused by the untreated effluents released by many companies, which contain hazardous materials like pesticides, wood preservatives, medicines, and petrochemicals. Nitro phenols (NPs), such as 2-nitrophenol (2-NP) and 4-nitrophenol (4-NP), are known to provide serious health dangers. They can cause symptoms such as cyanosis, burns to the skin and eyes, and confusion[1] As a result, it is imperative that NPs be removed from contaminated water. Many methods, such as adsorption, membrane filtering, chemical reduction, and degradation, have been studied for the removal of NPs.[2,3,4,5] Advanced oxidation processes, or AOPs, have become more significant in wastewater treatment in recent decades because of their capacity to decompose contaminants into innocuous chemicals like CO2 and H2O, particularly when light is present. Researchers' main focus has been on photocatalysis, particularly in the case of metal oxide or metal oxide hybrids. This method provides a reasonably efficient, economical, and ecologically beneficial way to get rid of organic contaminants.[6,7] The semiconductor known as CuO is recognized for its remarkable physicochemical properties, which include stability, a wider band gap (2.2 eV), photovoltaic capabilities, high-temperature superconductivity, and affordability. It is widely used in gas sensors; batteries, energy storage, and catalysis.[8, 9, 10] There are numerous ways to synthesize CuO nanoparticles, including high-temperature burning, novel rapid precipitation methods, son chemical and electrochemical procedures, and more. The goal of this work is to remove 2- and 4-

http://doi.org/10.31788/RJC.2024.1738865

nitrophenols from wastewater by employing a hydrothermally generated CuO/RGO binary composite. Furthermore, the study looks into the composite's antibacterial qualities. This binary nanocomposite was synthesized using a simple, environmentally benign hydrothermal method. A range of characterization methods were utilized to examine the structural and optical characteristics of the synthesized composite, including XRD, FTIR, FESEM-EDS, TEM, UV-DRS, PL, and TGA.[11,12,13,14,15,16] When evaluating the photocatalytic efficacy, model dye pollutants (NPs) were degraded in the presence of visible light, and Bacillus subtilis was used to gauge the antimicrobial activity.

EXPERIMENTAL

Synthesis of CuO/RGO Nanocomposite

In a streamlined production process is shown Fig.-1, 50 mg of pre-prepared graphene oxide (GO) was subjected to a 10-minute sonication method. Next, a Teflon beaker was used to mix 30 mL of 0.01 MCu $(CH_3COO)_2$ and 30 mL of 1 M NaOH aqueous solutions. The mixture was sealed and autoclaved at 180°C for three hours. The finished product was dried for a whole night at 70°C after filtration.

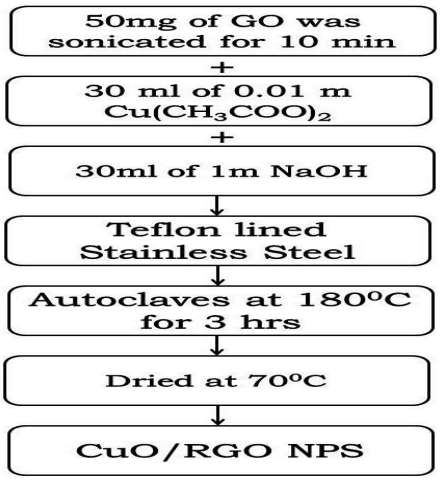

Fig.-1: Synthesis of CuO/RGO Nanocomposite

X-ray Diffraction

The resulting products exhibit a characteristic X-ray diffraction pattern, as shown in Fig.-2, with three distinct peaks at 2θ = 35.8, 39.2, and 62.01°. These peaks correspond to the (002), (200), and (113) planes of monoclinic CuO (JCPDS 45-0397). Crucially, the data show that there are pure CuO peaks because there are no impure peaks from Cu or Cu2O. These results strongly imply that the hydrothermal method of preparing CuO and CuO/RGO samples was successful. The synthesized Nano-composite's average crystallite size is calculated using Debye-Scherrer's formula, as expressed in Eqn.-1.

$$D = \frac{k\lambda}{\beta \cos\theta} \qquad (1)$$

In the framework of the Debye–Scherrer's formula (Eq.-1), the particle size ('D', in nm) is determined using the constants 'k' (set at 0.94), X-ray radiation wavelength ('λ' = 1.5406 Å), full-width at half maximum of the peak ('β', in radians), and Bragg angle ('2θ', in degrees). The calculated crystalline size of the composite is 19.3 nm. Significantly, this value is smaller than the crystalline size of CuO nanoparticles, which measures 29.6 nm.

Fourier Transform Infrared Spectroscopy (FTIR)

Fig.-3 shows FTIR spectra highlight distinctive characteristics. Notably, the generated material exhibits a monoclinic CuO structure as seen by two notable peaks at 540 and 604 cm^{-1}. Two faint peaks are also visible at 1129 and 1429 cm^{-1}; these are explained by the carboxylate ion's C=O stretching when it is bound to the CuO nanoparticles. Both spectra

show a large peak between 3074 and 3425 cm^{-1}, which is indicative of the existence of hydroxyl ions connected to the Cu-OH layer. Additionally, the hydrothermal approach maintains the equilibrium of water levels in CuO formed by the hydrothermal method by guaranteeing constant water content before and after the reaction, as shown by this broad peak. The identical peaks observed in both CuO and CuO/RGO nanocomposite suggests that the presence of GO loading does not exert any discernible effect on the structure of CuO.

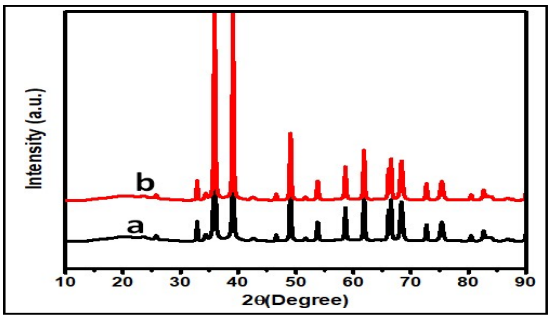

Fig.-2: XRD patterns of (a) CuO and (b) CuO / RGO NC

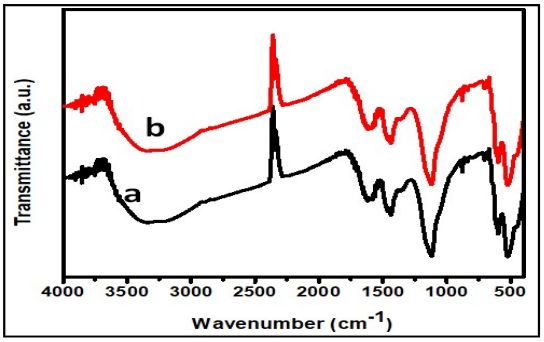

Fig.-3: FTIR Spectra of Prepared (a) CuO and (b) CuO /RGO NC

Morphology

Figures-4(a-b) and Fig.-4(c-d) illustrate the morphological details of CuO, which was synthesized using the hydrothermal process, at different magnifications. Additionally, Fig.-4(e) shows an EDS picture of the as-synthesized CuO/RGO nanocomposite.

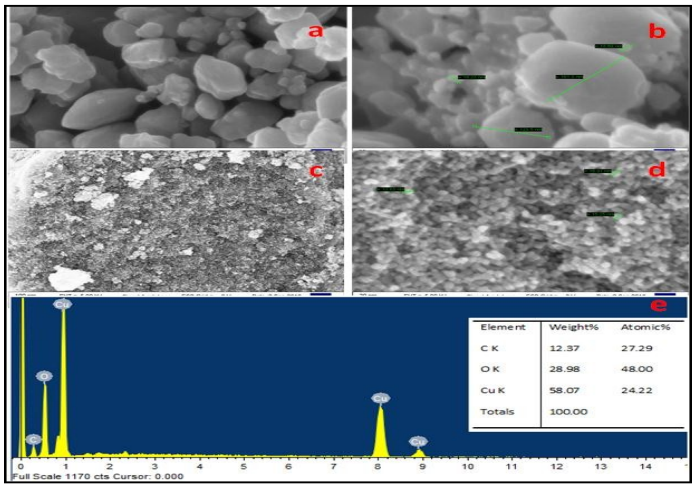

Fig.-4: FESEM Images were Captured for (a-d) CuO, (c-d) CuO/RGO Nanocomposite, and (e) the EDS Image of the Composite

The results show that this homogeneous structure contains copper (24%), oxygen (48%), and carbon (27%), with an atomic ratio of 1:2:1. This finding confirms the existence of the CuO/RGO composite.[16]However, the addition of silver and iron oxide caused noticeable clumping in the composite materials. The produced Nano-composite morphology was next examined under a TEM at magnifications of 50 and 100 nm, as shown in Fig.-5.

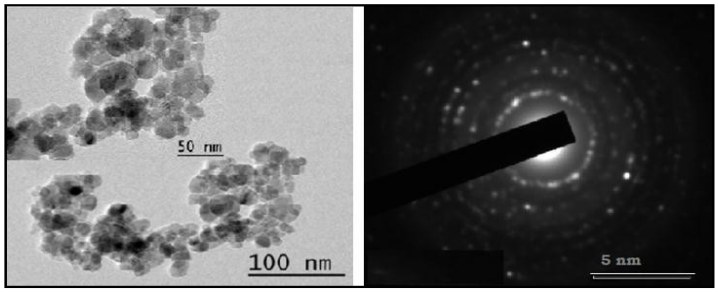

Fig.-5: TEM and SAED Images of Prepared CuO/RGO Composite

Ultraviolet Diffused Reflectance Spectroscopy (UV-DRS)

The absorption data was graphed as α^2E^2 versus E to generate the Tauc plot and Eqn.-2, facilitating the estimation of the band gap energies for the prepared materials.

$$(\alpha E)^2 = A(E - E_g) \qquad (2)$$

For semiconducting materials, the Tauc plot involves graphing $(\alpha E)^2$ against photon energy. At the locations where the two extrapolated lines cross the X-axis, the direct and indirect bandgap energies are found. In the case of CuO, the estimated bandgap energy is found to be 2.27 eV, while for the CuO/RGO nanocomposite, it is measured to be 2.08 eV. This is shown in Fig.-6.

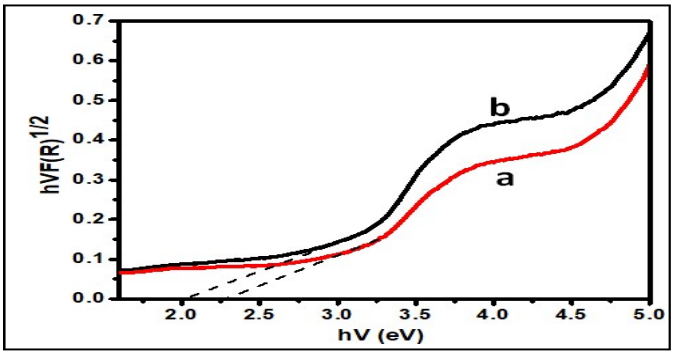

Fig.-.6: UV-DRS Spectra for (a) CuO and (b) CuO/RGO Nanocomposite

RESULTS AND DISCUSSION

Photo-catalytic Activity

To evaluate the photocatalytic activity of the prepared nanocomposite, tests were conducted using nitrophenols (ortho and para). The initial step involved examining the pH of the pollutant solution (4-NP) in both acidic and basic media. Significantly, at a pH of 8.1, the nanocomposite demonstrated the highest degradation of the pollutant under visible light illumination, as depicted in Fig.-7(b). The composite achieved complete degradation of 4-NP, surpassing pure CuO, which degraded 72% of 4-NP (Fig.-7(a)). This experiment highlights the enhanced performance of the composite.

Furthermore, the photocatalytic efficiency of the prepared composite was evaluated on 2-NP under visible light irradiation. The experimental conditions, including pH and the pollutant solution, were maintained consistently with those used for the 4-NP pollutant, ensuring a uniform approach throughout the experiment. The composite achieved complete degradation of 2-NP within 180 minutes, whereas CuO exhibited lower photocatalytic

degradation (68%), as illustrated in Fig.-8(a-b). This disparity in results emphasizes the superior photocatalytic performance of the composite compared to CuO.

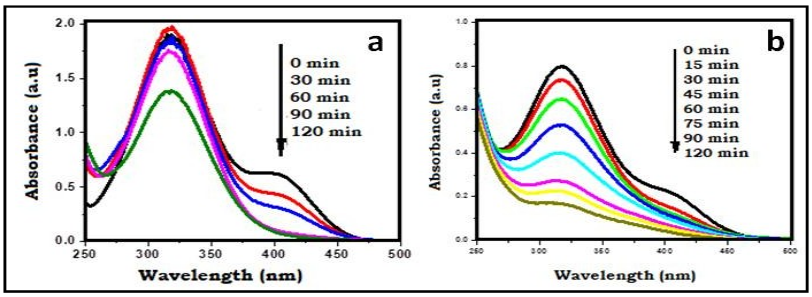

Fig.-7: Photocatalytic Degradation of 4-NP by (a) CuO and (b) CuO/RGO Composite

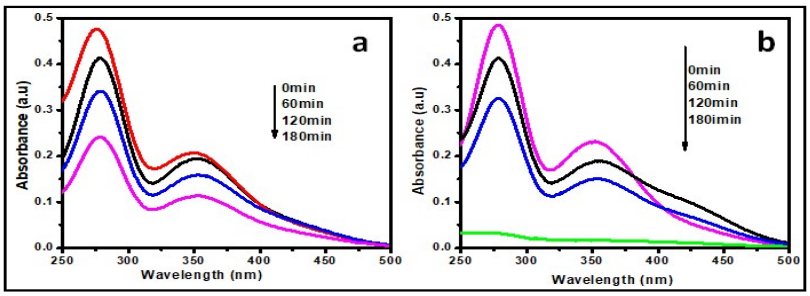

Fig.-8: Photocatalytic Degradation of 4-NP by (a) CuO and (b) CuO/RGO Composite

The peak absorption wavelengths for 4-nitrophenol (4-NP) and 2-nitrophenol (2-NP) were identified at 318 nm and 353 nm, respectively. Upon exposure to light, there is a reduction in absorption, leading to the transformation of the solution into a colorless state. The results unequivocally demonstrate that the CuO/RGO composite, synthesized via a hydrothermal route, effectively degrades both 10 mg/L 4-NP and 2-NP within 2 to 3 hours under visible light illumination. Notably, 4-NP exhibited a faster degradation rate compared to 2-NP when exposed to the synthesized composite. Because of its lower band gap than pure CuO, the produced composite is a very effective photocatalyst for the degradation of nitrophenols in the presence of visible light. Typically, CuO Nanomaterials demonstrate efficient visible-light-driven photocatalysis by generating electron-hole pairs. However, the narrow band gap of CuO results in a faster electron-hole recombination rate, leading to moderate photo-catalytic activity. To address this limitation, graphene oxide (GO) was loaded to form the CuO/RGO nanocomposite, exhibiting excellent photocatalytic efficiency. This enhancement is attributed to the efficient electron capture from the CuO conduction band by reduced graphene oxide (RGO). By inhibiting the recombination of electron-hole pairs, this action promotes increased electron transport and catalytic activity throughout the photo degradation process. The generated CuO/RGO composite provided an instructive illustration of the possible mechanism governing the photocatalytic destruction of organic contaminants under visible light irradiation.

Photoluminescence (PL) Spectra

In the domain of photocatalysis, hydroxyl radicals (•OH) assume a vital role as reactive species responsible for oxidation reactions. Given their high reactivity and brief lifespan, directly detecting hydroxyl radicals poses challenges. To evaluate the generation of hydroxyl radicals, the Photoluminescence (PL) technique was utilized. Coumarin, an organic compound, functioned as a fluorescent probe, engaging with hydroxyl radicals to produce 7-hydroxycoumarin.14 To do this, 0.10 g of the catalyst was dispersed and exposed to light in a 100 mL acidic solution containing 10 ppm of coumarin. 30-minute intervals were used to extract small samples of the reaction solution, filter them, and measure the photoluminescence intensity in the 350–600 nm range using an excitation wavelength of 435

nm. Fig.-9 displays the photoluminescence spectra of the 7-hydroxycoumarone that was generated, with a peak emission at 450 nm. Between 440 and 460 nm is where they are noticed. The photoluminescence intensity increased linearly with increasing irradiation periods. Nevertheless, no maximum excitation for the sample is shown in the absence of radiation (0 min in Fig.-10).

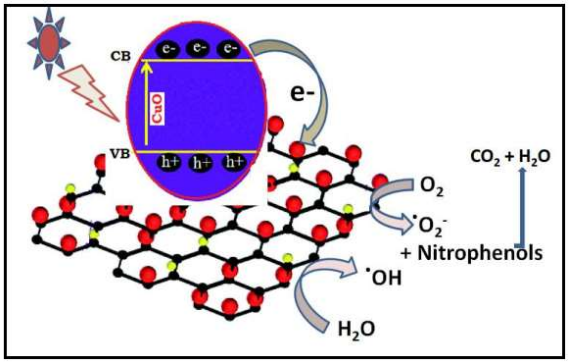

Fig.-9: Possible Mechanism for Photo Catalysis

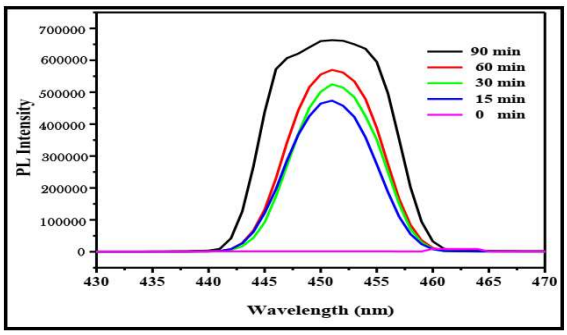

Fig.-10: PL Spectra of Prepared CuO/RGO Composite

It was found that there was a direct proportionality between the amount of hydroxyl radicals that formed on the catalyst surface and the length of time exposed to radiation. The findings provide more evidence that the CuO/RGO composite shows an increased rate of hydroxyl radical production when exposed to visible light. The pre-existing photo holes in the co-doped TiO_2 valence band are responsible for this enhancement because they can react directly with H_2O/OH- to produce hydroxyl radicals.

Antimicrobial Activity

The generated Nano-composite's antibacterial activity was assessed using the agar well diffusion method against Gram-positive (B. subtilis) and Gram-negative (E. coli) bacteria. The zone of inhibition (mm) that the CuO/RGO combination showed at various doses is detailed in Table-1. The findings clearly show that the produced composite has a more powerful inhibitory effect on the Gram-negative bacterium than it does on the Gram-positive equivalent. In particular, the CuO/RGO composite that was synthesized showed a zone of inhibition that measured 18 mm, 16 mm, and 15 mm for B. subtilis and 21 mm, 19 mm, and 18 mm for E. coli, respectively. Relevant literature supports the idea that copper's presence is responsible for this antibacterial activity shown in Fig.-11.

Table-1: Zone of Inhibition (mm) by CuO/RGO Composite

Organism	Test Compound	25mg/ml	10mg/ml	5mg/ml	Standard 10mg/ml
B.*subtilis*	CuO	10	9	9	32
	CuO/RGO	18	16	15	32
E.*coli*	CuO	14	13	12	32
	CuO/RGO	21	19	18	32

The composite exhibited strong antibacterial activity and is more advantageous than the CuO nanoparticles against bacterial strains tested.

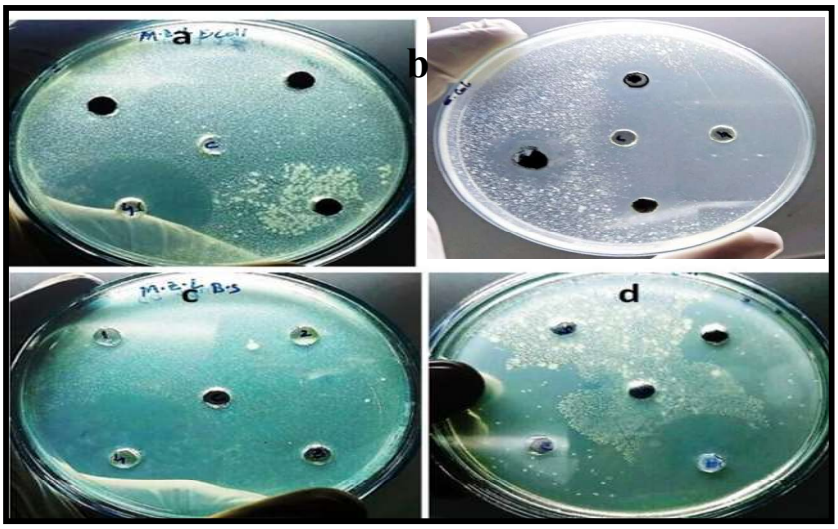

Fig.11: Antimicrobial Activity of CuO and CuO/RGO

CONCLUSION

An easy, solvent-free, and environmentally safe hydrothermal method was used to create the CuO /RGO nanocomposite, which is used in the photocatalytic degradation of pollutants, specifically 2-nitrophenol (2-NP) and 4-nitrophenol (4-NP)when exposed to visible light. The structure and morphology of the composite were investigated using FESEM and HRTEM, and the presence of Cu, O, and C was verified by elemental analysis using EDS. The FTIR spectra of the composite revealed distinct peaks in the 600–400 cm^{-1} range, indicating the existence of monoclinic CuO in the substance. Notably, the results demonstrated that the composite exhibited superior photocatalytic activity compared to pure CuO in visible light. This increase was attributed to the lower band gap of the composite, which stopped electron-hole pairs from recombining. Additionally, the composite's antibacterial activity was evaluated.

ACKNOWLEDGMENTS

The authors are thankful to the Inorganic Chemistry Laboratory, Andhra University, and Visakhapatnam, India for providing the synthesis facilities and nanotechnology lab, and to AU College of Engineering (A) for providing the characterization analysis.

CONFLICT OF INTERESTS

The authors declare that there is no conflict of interest regarding the publication of this article.

AUTHOR CONTRIBUTIONS

All the authors contributed significantly to this manuscript, participated in reviewing/editing and approved the final draft for publication. The research profile of the authors can be verified from their ORCID ids, given below:

Ravi Kota http://orchid.org/0009-0005-5550-8914
JayaRangaRaoPrathipati http://orchid.org/0000-0001-8561-1334
Matcha. Sowbhagya Lakshmi http://orchid.org/0009-0004-3973-4498
Yaddanapudi Venkata Bhaskara Lakshmi http://orchid.org/0000-0002-8845-9224
Narasimhulu Tamminana http://orchid.org/ 0000-0003-1519-0030

REFERENCES

1. Zhaokun Xiong, et al., *Chemical Engineering Journal*, **359**, 13(2019), https://doi.org/10.1016/j.cej.2018.11.111
2. Malgorzata Wasilewska, et al., *Journal of Environmental Chemical Engineering*, **9(4)**, 105459(2021), https://doi.org/10.1016/j.jece.2021.105459
3. A. G. Ramu, et al., *Chemosphere,* **271**, 129475(2021), https://doi.org/10.1016/j.chemosphere.2020.129475
4. Matthew A. Adebayo and Felicia I. Areo, *Resources, Environment and Sustainability,* **3**, 100020(2021), https://doi.org/10.1016/j.resenv.2021.100020
5. Jia-Qing Chen, et al., *Analytical Chemistry*, **94(5)**, 2517(2022), https://doi.org/10.1021/acs.analchem.1c04406
6. Siyuan Fang, and Yun Hang Hu, *Chemical Society Reviews*, **51**, 3609(2022), https://doi.org/10.1039/D1CS00782C
7. Li Xinru, et al., *Chem Catalysis*, **2(6)**, 1315(2022), https://doi.org/10.1016/j.checat.2022.04.007
8. Shahroz Saleem, et al., *Nanotechnology Reviews*, **11(1)**, 1 (2022), https://doi.org/10.1515/ntrev-2022-0473
9. R. Vandamar Poonguzhali, et al., *Ceramics International*, **48(18)**, 26287(2022), https://doi.org/10.1016/j.ceramint.2022.05.311
10. Jerry O.Adeyemi, Damian C. Onwudiwe, and Adebola O. Oyedeji, *Molecules,* **27(10)**, 3206(2022), https://doi.org/10.3390/molecules27103206
11. Hala M. Abo-Dief, et al., *Crystals*, **12(10)**,1423(2022), https://doi.org/10.3390/cryst12101423
12. R. M. Shah, , et al. *Materials Today: Proceeding,* **57(3)**, 1123(2022), https://doi.org/10.1016/j.matpr.2021.09.495
13. P. Joselene Suzan Jennifer, et al., *Inorganic Chemistry Communications,* **146**, 110218(2022), https://doi.org/10.1016/j.inoche.2022.110218
14. Fanli Meng, et al., *Ceramics International*, **49(4)**, 5595(2023), https://doi.org/10.1016/j.ceramint.2022.10.174
15. Haineng Bai, et al., *Sensors and Actuators B: Chemical*, **393**, 134195(2023), https://doi.org/10.1016/j.snb.2023.134195
16. Elumalai Arulkumar, and Sethuramachandran Thanikaikarasan, *Journal of Alloys and Compounds,* **998**, 175008(2024), https://doi.org/10.1016/j.jallcom.2024.175008

[RJC- 8865a/2024]